Investigation of the Performance of an Inductive Seawater Conductivity Sensor

WU Sheng, LAN Hui, LIANG Jin-Jin, TIAN Yu, DENG Yun, LI Hong-Zhi, LIU Ning

National Ocean Technology Center, No. 60 of Xian Yang road, 300112 Tian Jin, China
Tel.: +86)22-87862059, fax: +86 22-27536536
E-mail: olivier_wu9201@163.com

Abstract: As one of the factors in marine hydrographic survey, seawater salinity plays an important role in marine scientific research, marine exploitation and military defense. In practical measurement, the salinity is always presented indirectly by seawater conductivity value. Compared with the electrode conductivity sensors, inductive conductivity sensors have an advantage of anti-biofouling, and that is very interested in long term ocean observation device. From the principle point of view, this paper discus the different methods to improve inductive sensor output signal, which is confirmed by the relative experimental results. The basic working system of inductive sensor is described here as well as a calibration in standard seawater. From a wide range of temperature, measurement absolute error and stability are close to those of actual electrode conductivity sensors. Furthermore, in the 1000 meters deep sea experiment, our inductive sensor presents a perfect similarity of conductivity profile like sea-bird sensor, even for some small variations. The performance of our inductive sensor can compete with that of commercially available electrode conductivity sensors. *Copyright © 2015 IFSA Publishing, S. L.*

Keywords: Salinity measurement, Conductivity measurement, Electrode sensor, Inductive sensor, Temperature drift.

1. Introduction

Salinity is an important factor that provides the key information in oceanography. For example, a sudden change in salinity can destroy the coral reefs, which is caused by the climate change [1]. The salinity profile of the ocean is helpful to understand the fluctuations in seawater cycle [2]. Long term seawater salinity in fixed sea area is very useful for the marine monitoring, marine exploitation and military defense [3]. Conductivity measurement is the popular method to describe the salinity of seawater, which is principally performed by contact-

style sensor and inductive-style sensor. The contact sensors consist of two-electrode, three-electrode, four-electrode and seven-electrode sensors [4-5]. With no bare metal directly touching the seawater, inductive sensors have an advantage over those with electrodes, as electrodes are affected by polarization and fouling [6]. Inductive sensors can work more long than electrode sensors in seawater, which is considered as high efficiency devices in marine research domain [7]. In recent years, with the development of new material and integrated device electronics, this inductive sensor makes a rapid progress in its performance.

In this paper, details about inductive cell model are presented in Section 2. In Section 3, the optimization of output signal is shown, and a series of experiments have been performed to discuss the effect of inductive model parameters. The performance of inductive sensor from a wide range of temperature calibration in standard seawater is given in Section 4, and the conductivity measurement profile in 1000 meters deep sea is finally presented and compared with sea-bird sensor.

2. Inductive Cell Model

The inductive cell consists of two symmetrical toroids, which are considered as an excited and a received transformer respectively. Between two toroids, there is a seawater resistance loop. Fig. 1 illustrates an equivalent circuit that is used to describe the inductive process. The primary toroid has an inductance L_1 and the secondary toroid has an inductance L_3. Input excited alternating current I_1 flows in primary transformer and induces a magnetic loop l_2 and an inductive voltage V_2 in seawater resistance R_2. The secondary transformer receives the magnetic flux from seawater loop and gives an inductive voltage V_3.
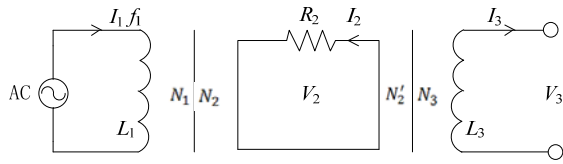

Fig. 1. Equivalent schematic of the inductive cell model.

As a transformer, a doughnut-shaped core wound with coil presents an inductance L (shown in Fig. 2), which can be calculated as:

$$L = \frac{\mu N^2 t}{2\pi} \ln \frac{r_2}{r_1},\tag{1}$$

where r_1 and r_2 are the internal and external radius respectively. r is the median radius, which should meet the relation $r_1 < r < r_2$. μ is the magnetic permeability. N is the turn number of coil. t is the thickness of core.

According to the Ampere's circuital theorem, the line integral of magnetic field $\vec{B_1}$ around the primary toroid magnetic loop l_1 is proportional to the total current $N_1 I_1$ (Seen in Equation (2)).

$$\oint_{l_1} \vec{B_1} \cdot d\vec{l_1} = \mu N_1 I_1,\tag{2}$$

In this equation, l_1 is equal to $2\pi r$ and $\vec{B_1}$ can be expressed by the following equation:

$$\vec{B_1} = \frac{\mu N_1 I_1}{2\pi r} \vec{e_\varphi},\tag{3}$$

where $\vec{e_\varphi}$ is the standard vector in cylindrical axis. Based on law of electromagnetic induction, the voltage in seawater resistance V_2 can be written as the integral of complex form:

$$V_2 = j\omega N_2 \iint_{S_1} \vec{B_1} \cdot d\vec{S}\tag{4}$$

S_1 is defined as the cross-sectional area of primary toroid, which is expressed as:

$$S_1 = 2\pi t \int_{r_1}^{r_2} dr\tag{5}$$

From the Equations (3) and (5), V_2 can be calculated as:

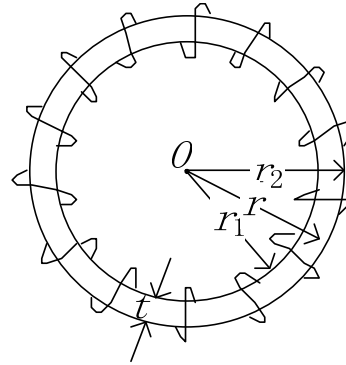$$V_2 = \frac{-j\omega\mu N_1 I_1 t}{2\pi} \ln \frac{r_2}{r_1}\tag{6}$$

Fig. 2. Equivalent toroid wound with coil.

The inductive current in seawater I_2 is obtained by V_2/R_2, where R_2 should conform to the Ohm theorem.

$$R_2 = \frac{l_2}{\sigma S_2}\tag{7}$$

S_2 is the cross-sectional area of seawater, which is determined by the structure of tube. σ is the conductivity of seawater. The formula of I_2 is presented as:

$$I_2 = \frac{-j\omega\mu N_1 I_1 t}{2\pi} \ln \frac{r_2}{r_1} \frac{S_2}{l_2} \sigma\tag{8}$$

In the manner of Equation (6), the complex voltage in secondary toroid V_3 is calculated as:

$$V_3 = \frac{-j\omega\mu N_3 I_2 t}{2\pi} \ln\frac{r_2}{r_1} \qquad (9)$$

If I_2 is replaced by the Equation (8), the value of output voltage in secondary toroid can be written as:

$$V_3 = \frac{-\omega^2 I_1 \mu^2 N_1 N_3 t^2}{4\pi^2}\left(\ln\frac{r_2}{r_1}\right)^2 \frac{S_2}{l_2}\sigma \qquad (10)$$

With the Formula (1), the Equation (10) is simplified as:

$$V_3 = \frac{-\omega^2 I_1 S_2 L_1 L_3}{l_2 N_1 N_3}\sigma \qquad (11)$$

Finally, it is found that the conductivity of seawater σ is linear proportional to output voltage V_3. This relation between two variables is determined by the physical parameters of inductive cell model. In order to obtain a high resolution, the possible solution is that increase the inductances L_1 and L_3, which can cause a high value of magnetic permeability. On the other hand, the moderate increase of excited current I_1 and frequency f ($\omega = 2\pi f$) can also be helpful. The other methods, for example, reduce the seawater magnetic loop l_2 and increase the surface S_2 are not discussed in this paper.

In next section, a discussion about the optimization of output voltage V_3 has been performed, which is confirmed by a series of experiments.

3. Discussion of Parameters

In our experiment, the inductive core has 10 mm thickness. 10 mm and 15 mm are the internal and external radius respectively for toroid. The seawater flows in a 48 mm length ceramic tube, which has a 5.75 mm radius and 104 mm equivalent loop. The turn of coil $N_1:N_2$ is chosen by 50:1 and $N_2:N_3$ is 1:200.

Applying the excited AC current $I_1 = 25$ mA and frequency $f_1 = 6$ kHz, the material of inductive core is replaced by soft magnetic ferrite alloy (Mn-Zn) and nanocrystalline soft magnetic alloy ($Fe_{72.8}Cu_{0.6}Nb_{2.6}Si_{15}B_9$) respectively. Fig. 3 and Fig. 4 illustrate the output voltage V_3 as function of seawater conductivity.

From the measured results, both conductivity values are linear proportional to output voltage V_3, These conductivity values are comparable to the results from theoretical calculation. However, for the same of seawater conductivity, the magnitude of V_3 in Fig. 4 is higher than that in Fig. 3. This multiple relation is from the magnetic permeability difference between $Fe_{72.8}Cu_{0.6}Nb_{2.6}Si_{15}B_9$ alloy (relative permeability $\mu_{eff} = 160000$) and Mn-Zn alloy (relative

permeability $\mu_{eff} = 15000$). The higher output voltage can achieve a better resolution, which is less affected by the noise.
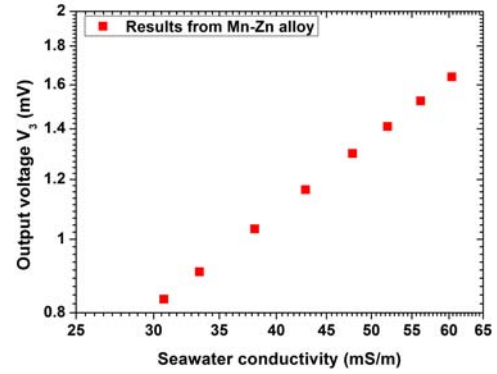

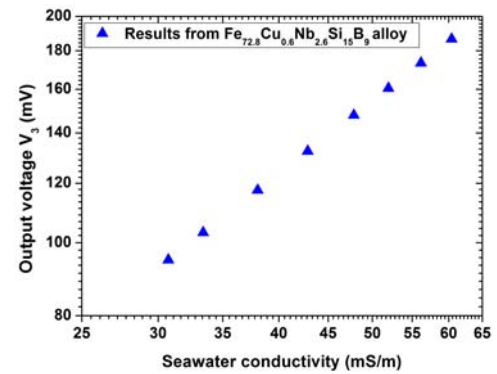**Fig. 3.** Conductivity measurement from soft magnetic ferrite alloy (Mn-Zn) core.

Fig. 4. Conductivity measurement from nanocrystalline soft magnetic alloy ($Fe_{72.8}Cu_{0.6}Nb_{2.6}Si_{15}B_9$) core.

Fig. 5 shows a variation of V_3 by regulating the excited current I_1. From 25 mA to 175 mA, it is found that an exact linear proportional relation between I_1 and V_3. However, due to the coil current dependence of loss, heat energy between winding coils can bring the change of permeability of soft magnetic material core [8]. This temperature drift can directly lead to a slowly increase of V_3.
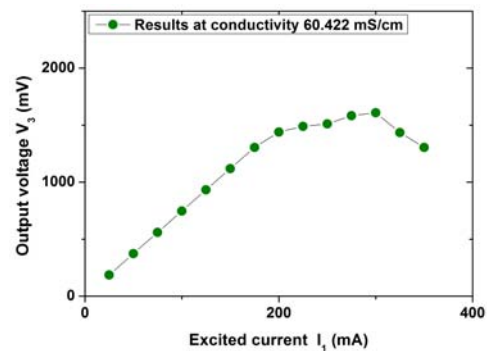

Fig. 5. Measured V_3 for excited current I_1.

After an excited current limit (about 300 mA), the coil can't match the inductive voltage. The temperature dependence of loss dominates the total inductive process, which causes V_3 to decrease [9].

According to the above discussion, it is necessary to compensate this temperature drift effect. A solution of system design is detailed in the following section.

Fig. 6 shows that V_3 versus excited frequency f_1. V_3 is not linear proportional to the frequency. That is because the permeability of soft magnetic material is not linearly varied with frequency. With increase of frequency, the hysteresis loss, eddy current loss and residual core loss in magnetic core [10-12] is not negligible, which bring a fall of sensor performance. In conclusion, the frequency should match the inductive core material in order to achieve the maximum permeability.
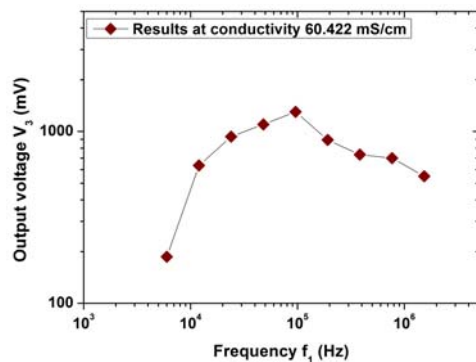
Fig. 6. Measured V_3 for excited frequency.

4. Experiment of System Performance

The schematic of inductive conductivity sensor is presented in Fig. 7. The excited current and frequency is controlled by a MCU chip, which aim at the output signal matching. After the signal amplification, a negative feedback and a regulator are applied to eliminate the effect of temperature drift. Passing an AC-DC conversion, this compensated signal is exported to PC terminal by RS232 interface. The signal processing is operated by the other MCU chip. The use of two MCU chips is not only increase data transmission rate, but also is very convenient to be integrated with the other sensors.

This inductive conductivity sensor is calibrated using standard seawater samples in the laboratory and the temperature is controlled by water bath. The first measurement results are presented in Table 1. It is found that most of conductivity absolute errors are less than 0.0003 mS/cm except the value at the temperature 27.99863 °C and 23.91047 °C. Table 2 shows that a repetition of calibration in six months. The stability of our inductive sensor is less than 0.00759 mS/cm for six months. Based on experimental results, our inductive sensor can meet exactly the seawater conductivity precision measurement need.
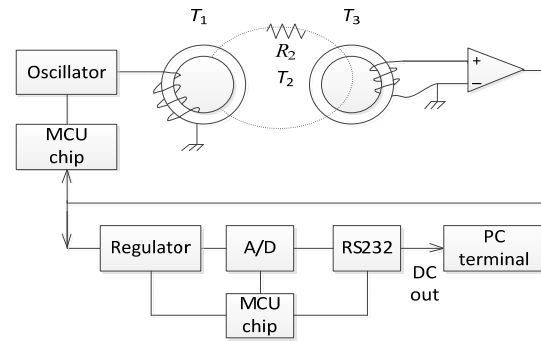

Fig. 7. Schematic of toroidal coil conductivity sensor.

Table 1. Calibration of inductive conductivity sensor in March 1, 2014. T_1 is the standard temperature, SC_1 is the standard conductivity, MC_1 is the measurement conductivity and AE is the absolute error (at standard salinity: 34.90142).

T_1 (°C)	SC_1 (mS/cm)	MC_1 (mS/cm)	AE (mS/cm)
31.99954	60.35278	60.3529	0.00010
27.99863	56.08498	56.0846	0.00035
23.91047	51.80450	51.8049	0.00039
19.92028	47.71602	47.7160	0.00002
15.00209	42.80981	42.8095	0.00029
9.95845	37.95191	37.9520	0.00012
4.99902	33.36772	33.3673	0.00008
2.00556	30.70124	30.7012	0.00006

Table 2. Calibration of inductive conductivity sensor in September 1, 2014 (at standard salinity: 34.89985).

T_1 (°C)	SC_1 (mS/cm)	MC_1 (mS/cm)	AE (mS/cm)
31.99920	60.49139	60.4875	0.00386
27.90017	56.11116	56.1073	0.00381
23.89829	51.91365	51.9083	0.00535
19.93803	47.84647	47.8389	0.00758
14.98966	42.89917	42.8917	0.00749
9.99963	38.08090	38.0736	0.00726
4.88428	33.34382	33.3371	0.00673
1.94918	30.72501	30.7212	0.00382

A seawater conductivity measurement has been performed in South China Sea (shown in Fig. 8).

Fig. 8. Experiment of sensors in South China Sea (date: 13 November, 2014).

From the surface of seawater to 1000 meters deep sea, three sensors have been applied to compare their performances, including inductive Sensor 1, inductive Sensor 2 and Sea-Bird 19 (three-electrode commercially available sensor).
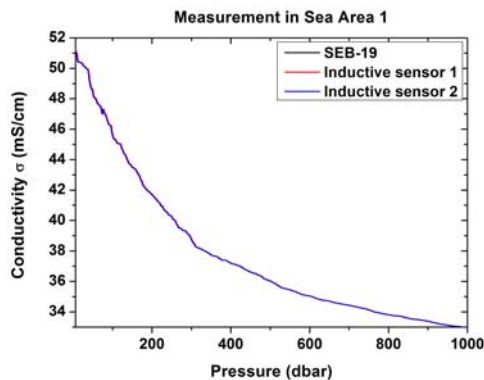

Fig. 9. Measured conductivity in 1000 m depth of seawater profile (data from sea area 1).
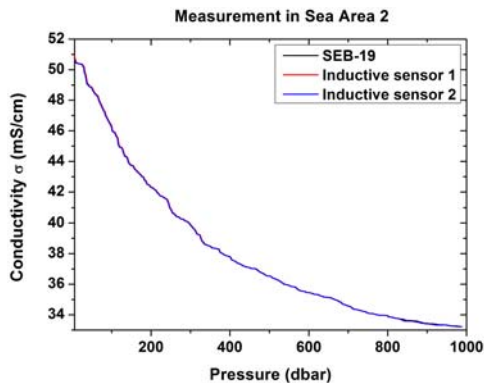

Fig. 10. Measured conductivity in 1000 m depth of seawater profile (data from sea area 2).

Fig. 9 and Fig. 10 illustrate seawater profile conductivity in two different sea areas. The variation of conductivity at shallow seawater is much higher than that at deep seawater, which is caused by the evident thermal energy exchange between the shallow seawater surface and atmosphere [13]. The measured conductivities from three sensors show an excellent dynamical similarity even for small variations. The performance of our designed inductive conductivity sensor is exactly close to that of sea-bird sensor.

5. Conclusions

In this paper, the principle of inductive conductivity sensor has been reported. It has been shown that a soft magnetic material with high permeability is required as inductive core to improve the sensor resolution. On the other hand, the appropriate change of excited current and frequency can be also useful for the optimization of sensor sensitivity. However, the temperature drift and magnetic loss should be taken into account, which can bring a fall of performance.

Using intelligent electronic circuit, our inductive sensor presents a small absolute error and high stability in calibration test. By comparing with electrode conductivity sensor in 1000 meters deep sea, our two experimental inductive sensors show an excellent similarity, which can be competed with the other commercially available sensor. This inductive sensor is possible to be integrated with fast perpendicular, plan and mobile marine carrier, which expand largely its long term application area.

Acknowledgements

References

[1]. Y. Yara, M. Fuji, H. Yamano, Y. Yamanaka, Projected coral bleaching in response to future sea surface temperature rises and the uncertainties among climate models, *Hydrobiologia*, Vol. 73, Issue 1, 2014, pp. 19-29.

[2]. K. Drushka, S. T. Gille, J. Sprintall, The diurnal salinity cycle in the tropics, *Journal of Geophysical Research: Oceans*, Vol. 119, Issue 9, 2014, pp. 5874-5890.

[3]. S. L. Wood, A. Nulph, B. P. Howell, Application of Autonomous Underwater Vehicles-Characterization of the Physical Environment for Development of Environment-Based Navigation Systems, *Sea Technology*, Vol. 45, Issue 12, 2004, pp. 10-14.

[4]. F. Laugere, G. W. Lubking, J. Bastemeijier, M. J. Vallkoo, Design of an electronic for capacitively coupled four-electrode conductivity detection in capillary electrophoresis microchip, *Sensors and Actuators B*, Vol. 83, 2002, pp. 104-108.

[5]. T. S. Light, S. Licht, A. C. Bevilacqua, K. R. Morash, The fundamental conductivity and resistivity of water, *Electrochemical and Solid-State Letters*, Vol. 8, Issue 1, 2005, pp. 16-19.

[6]. X. Hui, W. You, Z. Y. Luo, Y. W. Pan, A Miniature all-solid-state calcium electrode applied to *in situ* seawater measurement, *Measurement Science and Technology*, Vol. 24, Issue 12, 2013, pp. 5105-5109.

[7]. A. Fougere, New non-external field inductive conductivity sensor (NXIC) for long term deployments in biologically active regions, in *Proceedings of the IEEE Conference on Oceans 2000 MTS*, Providence, USA, 11-14 September 2000, pp. 623-630.

[8]. O. Inoue, N. Matsutani, K. Kugimiya, Low loss MnZn-ferrites: frequency dependence of minimum power loss temperature, *IEEE Transactions on Magnetics*, Vol. 29, Issue 6, 1993, pp. 3532-3534.

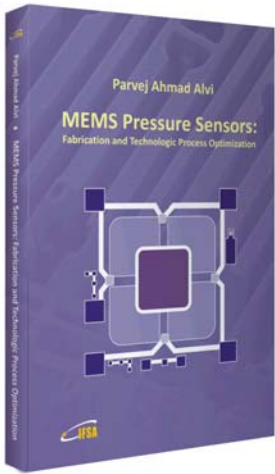[9]. P. J. Van der Zaag, New views on the dissipation in soft magnetic ferrites, *Journal of Magnetism and*

Magnetic Materials*, Vol. 196-197, 1999, pp. 315-319.

[10]. D. Stoppels, Development in soft magnetic power ferrites, in *Proceedings of the 12th International Conference on Soft Magnetic Materials*, Krakow, Poland, 12-14 September 1995, pp. 323-328.

[11]. W. Roshen, Ferrite core loss for power magnetic components design, *IEEE Transactions on Magnetics,* Vol. 27, Issue 6, 1991, pp. 4407-4415.

[12]. W. H. Jeong, Y. H. Ho, B. M. Song, Effects of grain size on the residual loss of Mn-Zn ferrites, *Journal of Applied Physics*, Vol. 91, Issue 10, 2002, pp. 7619-7621.

[13]. V. Kudryavtsev, B. Chapron, V. Makin, Impact of wind waves on the air-sea fluxes: A coupled model, *Journal of Geophysical Research: Oceans*, Vol. 119, Issue 2, 2014, pp. 1217-1236.

―――――――――――――